PIER C

(Received 3 August 2025, Accepted 23 January 2026, Scheduled 28 February 2026)

A Semi-Analytical Method for Calculation of Electromagnetic Fields in Horizontal Multilayered Media with Full Anisotropy

Guibo Chen* and Ye Zhang

School of Physics, Changchun University of Science and Technology, Jilin, China

ABSTRACT: In this paper, a semi-analytical method for the calculation of electromagnetic (EM) fields in horizontal multilayered media (HMLM) with full anisotropy is presented. First, the governing equation was obtained by the plane wave decomposition to Maxwell's equations, and the EM fields in the wavenumber domain (WD) were solved by means of eigensystems. Subsequently, a more intuitive derivation of the spectral-domain propagation matrix method based on existing literature was employed to calculate WD's EM fields in the HMLM. Finally, the EM fields in the spatial domain (SD) were obtained by 2-D inverse Fourier transform. To accelerate the evaluation of SD's EM fields, 2-D infinite integrals were transformed into semi-infinite integrals including sine(cosine) functions by Euler's formula, and fast sine(cosine) transforms based on digital filters were introduced. It has been shown that the proposed semi-analytical method can be effectively used to calculate the EM fields in HMLM with full anisotropy through the comparison with the existing numerical algorithm.

1. INTRODUCTION

Modeling of electromagnetic (EM) fields in horizontal multilayered media (HMLM) is widely used in antenna design, remote sensing, and geophysical prospecting [1–4]. Not only can it describe the fundamental physical processes of EM waves propagation, reflection, transmission, and attenuation in HMLM, but more significantly, it is also the basis and key part to solve the EM scattering problems of 3-D objects buried in HMLM by the Method of Moments (MOM) [5–12].

In the classical book by Chew [5], rigorous derivation processes were systematically introduced to calculate the EM fields in layered media with horizontal, cylindrical, and spherical configurations. Chew also presented dyadic Green's functions (DGFs) for EM fields in HMLM based on the vector wave function approach, along with their application in integral equation formulations for EM scattering by buried 3-D objects. In addition, there is a considerable body of literature on EM modeling in a horizontal-layered medium. For isotropic formation, Wannamaker et al. derived the expressions of EM fields and DGFs in the HMLM suitable for solving the 3-D geo-electric integral equation [7], and Lin et al. derived approximate formulas for the radiation EM fields excited by a vertical electric dipole in the presence of a four-layered region [13]. Okhmatovski and Zheng presented rigorous fundamental principles, mathematical derivations, numerical methodologies, and application areas of EM fields for layered media in their recently published book [14].

For a transverse isotropic formation, Kong solved the EM propagation problems for the HMLM by decomposing the field into different modes [15]. Michalski and Mosig provided compact representations of potential- and field-type DGFs for HMLM based on the Transmission-Line Network (TMLN) [16]. Chen et al. studied the singularity elimination of DGFs in HMLM and its applications in solving the 3-D contraction integral equation [12]. For an azimuthal anisotropic formation, Li and Pedersen developed methods to derive EM fields from a grounded dipole on half-space and HMLM, respectively [17, 18]. For orthotropic anisotropic formation, Li et al. proposed an analytical algorithm for EM fields excited by magnetic dipoles in HMLM using a classical propagator matrix [19]. For more complex anisotropic formations, Huang and Lee obtained the DGFs of EM fields for unbounded and two-layered general anisotropic media using the eigen-decomposition method [20], Yin and Maurer proposed a method suitable for the calculation of low-frequency EM induction in arbitrary anisotropic layered earth [21], and Løseth and Ursin studied the EM fields in symmetric anisotropic layered media [22]. For a full anisotropic formation, Hu et al. proposed a method to calculate EM fields in HMLM [23]. To our knowledge, there are relatively few works on the study of EM responses in HMLM with full anisotropy due to the mathematical complexity [24].

In this study, a semi-analytical method is proposed for the calculation of EM fields in HMLM with full anisotropy. Building on the spectral-domain propagator matrix method established in existing literature [22, 23], this study constructs recursive formulas by explicitly tracing the propagation and multiple-reflection paths of waves between layers, thereby making the derivation process of EM fields and generalized reflection coefficients in the wavenumber domain (WD) more intuitive while maintaining consistency in the mathematical framework. In addition, to accelerate the numerical evaluation of DGFs in the spatial domain (SD), a fast sine(cosine)

* Corresponding author: Guibo Chen (guibochen@cust.edu.cn).

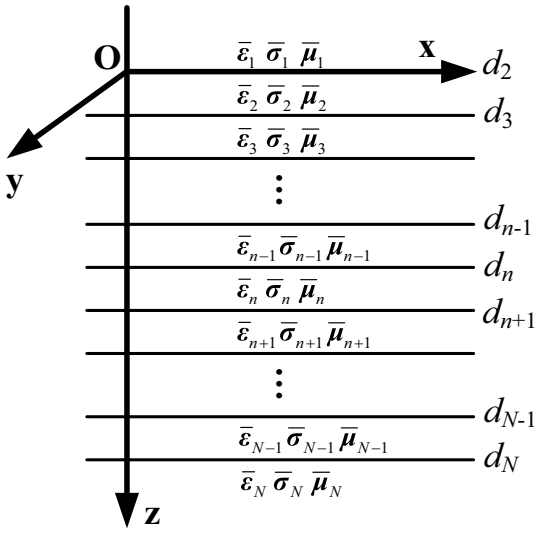

FIGURE 1. Model diagram of horizontal multilayered anisotropic medium.

transform algorithm based on digital filters was introduced, in contrast to the conventional direct quadrature used in existing literature.

The structure of this paper is as follows. In Section 2, physical modeling and EM solutions are presented, including the decomposition of Maxwell's equations, derivation of EM fields in the WD, reflection and transmission at the interface, analytical solutions of eigenvalues and eigenvectors, and evaluation of DGFs in the SD. In Section 3, the proposed method is verified by comparison with existing algorithms. Our main conclusions are summarized in Section 4.

2. PHYSICAL MODELING AND EM SOLUTIONS

2.1. Decomposition of Maxwell's Equations

Consider the HMLM model consisting of N layers separated by the horizontal interfaces parallel to the x-y plane of a Cartesian coordinate system and located at $z = d_2 d_3, \ldots, d_N$ as shown in Figure 1, the permittivity, conductivity, and permeability of each piecewise homogeneous region are assumed to be 3×3 tensor:

$$\bar{\boldsymbol{\varepsilon}} = \begin{bmatrix} \varepsilon_{xx} & \varepsilon_{xy} & \varepsilon_{xz} \\ \varepsilon_{yx} & \varepsilon_{yy} & \varepsilon_{yz} \\ \varepsilon_{zx} & \varepsilon_{zy} & \varepsilon_{zz} \end{bmatrix}, \quad \bar{\boldsymbol{\sigma}} = \begin{bmatrix} \sigma_{xx} & \sigma_{xy} & \sigma_{xz} \\ \sigma_{yx} & \sigma_{yy} & \sigma_{yz} \\ \sigma_{zx} & \sigma_{zy} & \sigma_{zz} \end{bmatrix}$$

$$\bar{\boldsymbol{\mu}} = \begin{bmatrix} \mu_{xx} & \mu_{xy} & \mu_{xz} \\ \mu_{yx} & \mu_{yy} & \mu_{yz} \\ \mu_{zx} & \mu_{zy} & \mu_{zz} \end{bmatrix} \tag{1}$$

There is an electric (magnetic) dipole source $\mathbf{J}(\mathbf{M})$ at $r' = (x', y', z')$ with a time dependence of $\exp(-i\omega t)$, which can generate EM fields at $r = (x, y, z)$ that satisfy Maxwell's equations [1]:

$$\begin{cases} \nabla \times \mathbf{E} = i\omega \bar{\boldsymbol{\mu}} \cdot \mathbf{H} - \mathbf{M} \\ \nabla \times \mathbf{H} = -i\omega \bar{\boldsymbol{\varepsilon}}^* \cdot \mathbf{E} + \mathbf{J} \end{cases} \tag{2}$$

where complex permittivity $\bar{\boldsymbol{\varepsilon}}^*$ can be expressed as $\varepsilon^*_{\xi\varsigma} = \varepsilon_{\xi\varsigma} - \frac{\sigma_{\xi\varsigma}}{i\omega}$ $(\xi, \varsigma = x, y, z)$.

Because the HMLM shown in Figure 1 holds an infinite range in the transverse direction, the following plane wave decomposition [25, 26]

$$\begin{aligned} &\tilde{f}(k_x, k_y; z, z') \\ &= \iint_{-\infty}^{+\infty} f(x-x', y-y'; z, z') \mathrm{e}^{-i\left[k_x(x-x')+k_y(y-y')\right]} dxdy \end{aligned} \tag{3}$$

can be applied to Eq. (2), and the governing equation of the EM fields in the WD can be obtained as

$$\left(\bar{\mathbf{I}} \frac{d}{dz} + i\bar{\mathbf{K}}\right) \boldsymbol{\Psi}(z) = \mathbf{s} \tag{4}$$

where k_x and k_y denote the wavenumbers in x- and y-directions; $\bar{\mathbf{I}}$ is the identity matrix; and $\boldsymbol{\Psi}(z)$ represents the transverse fields vector given by

$$\boldsymbol{\Psi}(z) = \left[\tilde{E}_x, \tilde{E}_y, -\tilde{H}_y, \tilde{H}_x\right]^{\mathrm{T}}. \tag{5}$$

In Eq. (4), source vector $\mathbf{s} = [s_1, s_2, s_3, s_4]^{\mathrm{T}}$ can be written as:

$$s_1 = \frac{k_x}{\omega \varepsilon^*_{zz}} \tilde{J}_z - \tilde{M}_y + \frac{\mu_{yz}}{\mu_{zz}} \tilde{M}_z \tag{6}$$

$$s_2 = \frac{k_y}{\omega \varepsilon^*_z} \tilde{J}_z + \tilde{M}_x - \frac{\mu_{xz}}{\mu_{zz}} \tilde{M}_z \tag{7}$$

$$s_3 = \tilde{J}_x - \frac{\varepsilon^*_{xz}}{\varepsilon^*_{zz}} \tilde{J}_z - \frac{k_y}{\omega \mu_z} \tilde{M}_z \tag{8}$$

$$s_4 = \tilde{J}_y - \frac{\varepsilon^*_{yz}}{\varepsilon^*_{zz}} \tilde{J}_z + \frac{k_x}{\omega \mu_z} \tilde{M}_z \tag{9}$$

and the coefficient matrix $\bar{\boldsymbol{K}}$ with 4×4 can be expressed as:

$$\bar{\mathbf{K}} = \begin{bmatrix} \bar{\mathbf{K}}_{11} & \bar{\mathbf{K}}_{12} \\ \bar{\mathbf{K}}_{21} & \bar{\mathbf{K}}_{22} \end{bmatrix} \tag{10}$$

$$\bar{\mathbf{K}}_{11} = \begin{bmatrix} \frac{\varepsilon^*_{zx} k_x}{\varepsilon^*_{zz}} + \frac{\mu_{yz} k_y}{\mu_{zz}} & \frac{\varepsilon^*_{zy} k_x}{\varepsilon^*_{zz}} - \frac{\mu_{yz} k_x}{\mu_{zz}} \\ \frac{\varepsilon^*_{zx} k_y}{\varepsilon^*_{zz}} - \frac{\mu_{xz} k_y}{\mu_{zz}} & \frac{\varepsilon^*_{zy} k_y}{\varepsilon^*_{zz}} + \frac{\mu_{xz} k_x}{\mu_{zz}} \end{bmatrix} \tag{11}$$

$$\bar{\mathbf{K}}_{12} = \begin{bmatrix} \omega\left(\mu_{yy} - \frac{\mu_{yz}\mu_{zy}}{\mu_{zz}}\right) - \frac{k_x^2}{\omega \varepsilon^*_{zz}} & \omega\left(\frac{\mu_{yz}\mu_{zx}}{\mu_{zz}} - \mu_{yx}\right) - \frac{k_x k_y}{\omega \varepsilon^*_{zz}} \\ \omega\left(\frac{\mu_{xz}\mu_{zy}}{\mu_{zz}} - \mu_{xy}\right) - \frac{k_x k_y}{\omega \varepsilon^*_{zz}} & \omega\left(\mu_{xx} - \frac{\mu_{xz}\mu_{zx}}{\mu_{zz}}\right) - \frac{k_y^2}{\omega \varepsilon^*_{zz}} \end{bmatrix} \tag{12}$$

$$\bar{\mathbf{K}}_{21} = \begin{bmatrix} \omega\left(\varepsilon^*_{xx} - \frac{\varepsilon^*_{xz}\varepsilon^*_{zx}}{\varepsilon^*_{zz}}\right) - \frac{k_y^2}{\omega \mu_{zz}} & \omega\left(\varepsilon^*_{xy} - \frac{\varepsilon^*_{xz}\varepsilon^*_{zy}}{\varepsilon^*_{zz}}\right) + \frac{k_x k_y}{\omega \mu_{zz}} \\ \omega\left(\varepsilon^*_{yx} - \frac{\varepsilon^*_{yz}\varepsilon^*_{zx}}{\varepsilon^*_{zz}}\right) + \frac{k_x k_y}{\omega \mu_{zz}} & \omega\left(\varepsilon^*_{yy} - \frac{\varepsilon^*_{yz}\varepsilon^*_{zy}}{\varepsilon^*_{zz}}\right) - \frac{k_x^2}{\omega \mu_{zz}} \end{bmatrix} \tag{13}$$

$$\bar{\mathbf{K}}_{22} = \begin{bmatrix} \frac{\varepsilon^*_{xz} k_x}{\varepsilon^*_{zz}} + \frac{\mu_{zy} k_y}{\mu_{zz}} & \frac{\varepsilon^*_{xz} k_y}{\varepsilon^*_{zz}} - \frac{\mu_{zx} k_y}{\mu_{zz}} \\ \frac{\varepsilon^*_{yz} k_x}{\varepsilon^*_{zz}} - \frac{\mu_{zy} k_x}{\mu_{zz}} & \frac{\varepsilon^*_{yz} k_y}{\varepsilon^*_{zz}} + \frac{\mu_{zx} k_x}{\mu_{zz}} \end{bmatrix} \tag{14}$$

If the solutions of $\boldsymbol{\Psi}(z)$ are obtained, then the vertical components can be calculated using the transverse fields:

$$\tilde{E}_z = \frac{1}{i\omega \varepsilon^*_{zz}} \left[ik_y \tilde{H}_x - ik_x \tilde{H}_y - i\omega \varepsilon^*_{zx} \tilde{E}_x - i\omega \varepsilon^*_{zy} \tilde{E}_y\right] \tag{15}$$

$$\tilde{H}_z = \frac{1}{i\omega \mu_{zz}} \left[ik_x \tilde{E}_y - ik_y \tilde{E}_x - i\omega \mu_{zx} \tilde{H}_x - i\omega \mu_{zy} \tilde{H}_y\right] \tag{16}$$

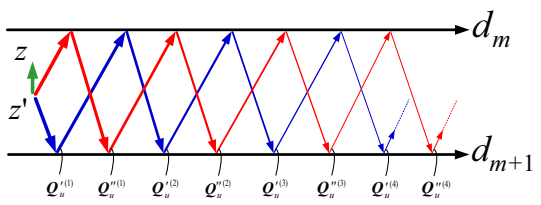

FIGURE 2. Schematic diagram of wave propagation when source and receiver are in the m-layer.

2.2. EM Fields in the WD

To solve Eq. (4), the coefficient matrix is diagonalized as $\bar{\mathbf{K}}=\bar{\mathbf{A}}\cdot\bar{\mathbf{\Lambda}}\cdot\bar{\mathbf{A}}^{-1}$, and Eq. (4) can be transformed into the following equation [27]:

$$\left(\bar{\mathbf{I}}\frac{d}{dz}+i\bar{\mathbf{\Lambda}}\right)\boldsymbol{\phi}(z)=\mathbf{S} \tag{17}$$

where,

$$\mathbf{S} = \bar{\mathbf{A}}^{-1}\cdot\mathbf{s} \tag{18}$$

$$\bar{\mathbf{\Lambda}} = \mathrm{diag}(\lambda_1,\lambda_2,\lambda_3,\lambda_4)=\begin{bmatrix}\bar{\mathbf{\Lambda}}_1 & \mathbf{0}\\ \mathbf{0} & \bar{\mathbf{\Lambda}}_2\end{bmatrix} \tag{19}$$

In (17)–(19), $\bar{\mathbf{A}}$ is the eigenvector matrix corresponding to $\bar{\mathbf{K}}$ and is formed by the set of eigenvectors as columns; $\bar{\mathbf{\Lambda}}$ is the diagonal matrix composed of eigenvalues of $\bar{\mathbf{K}}$; and $\boldsymbol{\phi}(z)$ is the unknown quantity containing the EM fields to be solved:

$$\boldsymbol{\phi}(z)=\bar{\mathbf{A}}^{-1}\cdot\mathbf{\Psi}(z) \tag{20}$$

To ensure numerical stability, among the four eigenvalues of $\bar{\mathbf{\Lambda}}$, the two with positive imaginary parts $\bar{\mathbf{\Lambda}}_1$ are designated as representing the contributions of up-traveling waves, whereas the two with negative imaginary parts $\bar{\mathbf{\Lambda}}_2$ represent the contributions of down-traveling waves. Then, $\boldsymbol{\phi}(z)$ and $\mathbf{S}$ can be expressed as the following combinations of up- and down-traveling waves:

$$\boldsymbol{\phi}(z) = \begin{bmatrix}\boldsymbol{\phi}_u & \boldsymbol{\phi}_d\end{bmatrix}^{\mathrm{T}} \tag{21}$$

$$\mathbf{S} = \begin{bmatrix}\mathbf{S}_u & \mathbf{S}_d\end{bmatrix}^{\mathrm{T}} \tag{22}$$

In a homogeneous medium, solutions of (17) can be given by:

$$\boldsymbol{\phi}_u^{(p)} = -\mathrm{e}^{i\bar{\mathbf{\Lambda}}_1^{(m)}(z'-z)}\cdot\mathbf{S}_u \qquad (z<z') \tag{23}$$

$$\boldsymbol{\phi}_d^{(p)} = \mathrm{e}^{-i\bar{\mathbf{\Lambda}}_2^{(m)}(z-z')}\cdot\mathbf{S}_d \qquad (z>z') \tag{24}$$

In the HMLM, solutions of (17) are obtained by the following three cases:

(1). The source and receiver are in the same layer (m-layer)

The case where $d_{\mathrm{m}} < z < z'$ shown in Figure 2 will be considered. Under this condition, the up-traveling waves are composed of direct waves and reflected waves (including multiple reflected waves) caused by the interfaces. Therefore, the up-traveling waves can be expressed as:

$$\boldsymbol{\phi}_u=\boldsymbol{\phi}_u^{(p)}+\boldsymbol{\phi}_u^{(s)} \tag{25}$$

where $\boldsymbol{\phi}_u^{(p)}$ indicates the primary wave propagating directly from z' to z, and $\boldsymbol{\phi}_u^{(s)}$ represents the contribution of reflected waves corresponding to boundary effects and can be written as [22]:

$$\boldsymbol{\phi}_u^{(s)}=\mathrm{e}^{i\bar{\mathbf{\Lambda}}_1^{(m)}(d_{m+1}-z)}\cdot\mathbf{Q}_u \tag{26}$$

where $\mathbf{Q}_u$ is defined as the amplitude of the up-traveling waves at interface d_{m+1}. As shown in Figure 2, the up-traveling waves at interface d_{m+1} are the results of the reflection of the down-traveling waves at the interface. Because $\mathbf{Q}_u$ contains multiple reflection processes, it can be decomposed into the following terms:

$$\mathbf{Q}_u=\mathbf{Q}_u^{(1)}+\mathbf{Q}_u^{(2)}+\mathbf{Q}_u^{(3)}+\ldots \tag{27}$$

Furthermore, for the first term $\mathbf{Q}_u^{(1)}$ in the above equation, the up-traveling wave consists of two parts. One is the down-traveling wave from z' propagating to interface d_{m+1} (i.e., the part in brackets [...] in (28)), which is then reflected to form the up-traveling wave $\mathbf{Q}'^{(1)}_u$. The second is that the up-traveling wave from z' propagates to the interface d_m (i.e., the part in $\langle\ldots\rangle$ in (29)), and then it is reflected to form the down-traveling wave (i.e., the part in [...] in (29)). This down-traveling wave propagates to the interface d_{m+1} (i.e., part of $\langle\ldots\rangle$ in (29)) and is reflected to form the up-traveling wave $\mathbf{Q}''_{u^{(1)}}$. The above physical process can be expressed using the following formulas,

$$\mathbf{Q}'_{u^{(1)}}=\tilde{\bar{\mathbf{R}}}_{m,m+1}\left[\mathrm{e}^{-i\bar{\mathbf{\Lambda}}_2^{(m)}\left(d_{m+1}-z'\right)}\cdot\mathbf{S}_d\right] \tag{28}$$

$$\mathbf{Q}''_{u^{(1)}}=-\tilde{\bar{\mathbf{R}}}_{m,m+1}\left\{\mathrm{e}^{-i\bar{\mathbf{\Lambda}}_2^{(m)}h_m}\left[\tilde{\bar{\mathbf{R}}}_{m,m-1}\left\langle\mathrm{e}^{i\bar{\mathbf{\Lambda}}_1^{(m)}(z'-d_m)}\cdot\mathbf{S}_u\right\rangle\right]\right\} \tag{29}$$

here, $h_m=d_{m+1}-d_m$ is the thickness of the m-th layer. From Figure 2, the second- and third-terms in (27) can be written as:

$$\mathbf{Q}_u^{(2)} = \tilde{\bar{\mathbf{R}}}_{m,m+1}\mathrm{e}^{-i\bar{\mathbf{\Lambda}}_2^{(m)}h_m}\tilde{\bar{\boldsymbol{R}}}_{m,m-1}\mathrm{e}^{i\bar{\mathbf{\Lambda}}_1^{(m)}h_m}\cdot\mathbf{Q}_u^{(1)} \tag{30}$$

$$\mathbf{Q}_u^{(3)} = \tilde{\bar{\mathbf{R}}}_{m,m+1}\mathrm{e}^{-i\bar{\mathbf{\Lambda}}_2^{(m)}h_m}\tilde{\bar{\boldsymbol{R}}}_{m,m-1}\mathrm{e}^{i\bar{\mathbf{\Lambda}}_1^{(m)}h_m}\cdot\mathbf{Q}_u^{(2)} \tag{31}$$

Considering (27)–(31), one can obtain:

$$\mathbf{Q}_u=\mathbf{Q}_u^{(1)}+\tilde{\bar{\mathbf{R}}}_{m,m+1}\mathrm{e}^{-i\bar{\mathbf{\Lambda}}_2^{(m)}h_m}\tilde{\bar{\mathbf{R}}}_{m,m-1}\mathrm{e}^{i\bar{\mathbf{\Lambda}}_1^{(m)}h_m}\cdot\mathbf{Q}_u \tag{32}$$

Substituting (28) and (29) into (32) yields the following expression for $\mathbf{Q}_u$:

$$\mathbf{Q}_u=\left[\bar{\mathbf{I}}-\tilde{\bar{\mathbf{R}}}_{m,m+1}\mathrm{e}^{-i\bar{\mathbf{\Lambda}}_2^{(m)}h_m}\tilde{\bar{\mathbf{R}}}_{m,m-1}\mathrm{e}^{i\bar{\mathbf{\Lambda}}_1^{(m)}h_m}\right]^{-1}\cdot\begin{bmatrix}-\tilde{\bar{\mathbf{R}}}_{m,m+1}\mathrm{e}^{-i\bar{\mathbf{\Lambda}}_2^{(m)}h_m}\tilde{\bar{\mathbf{R}}}_{m,m-1}\mathrm{e}^{i\bar{\mathbf{\Lambda}}_1^{(m)}\left(z'-d_m\right)}\cdot\mathbf{S}_u\\ +\tilde{\bar{\mathbf{R}}}_{m,m+1}\mathrm{e}^{-i\bar{\mathbf{\Lambda}}_2^{(m)}\left(d_{m+1}-z'\right)}\cdot\mathbf{S}_d\end{bmatrix} \tag{33}$$

The down-traveling waves can be written as:

$$\boldsymbol{\phi}_d=\mathrm{e}^{-i\bar{\mathbf{\Lambda}}_2^{(m)}(z-d_m)}\cdot\mathbf{Q}_d \tag{34}$$

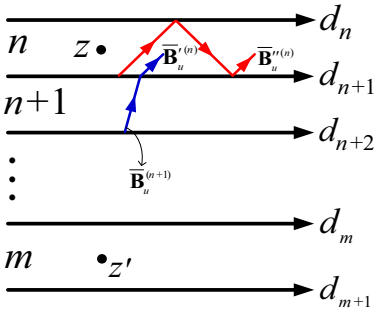

FIGURE 3. Schematic diagram of wave propagation when the source layer is below the receiver layer.

where $\mathbf{Q}_d$ represents the amplitude of the down-travelling waves at d_m. Similar to the derivation of $\mathbf{Q}_u$, $\mathbf{Q}_d$ can be expressed as:

$$\mathbf{Q}_d=\left\{\begin{bmatrix}\bar{\mathbf{I}}-\tilde{\bar{\mathbf{R}}}_{m,m-1}e^{i\bar{\mathbf{\Lambda}}_1^{(m)}h_m}\tilde{\bar{\mathbf{R}}}_{m,m+1}e^{-i\bar{\mathbf{\Lambda}}_2^{(m)}h_m}\end{bmatrix}^{-1}\right.\cdot\left[\begin{matrix}-\tilde{\bar{\mathbf{R}}}_{m,m-1}e^{i\bar{\mathbf{\Lambda}}_1^{(m)}\left(z'-d_m\right)}\cdot\mathbf{S}_u\\+\tilde{\bar{\mathbf{R}}}_{m,m-1}e^{i\bar{\mathbf{\Lambda}}_1^{(m)}h_m}\tilde{\bar{\mathbf{R}}}_{m,m+1}e^{-i\bar{\mathbf{\Lambda}}_2^{(m)}\left(d_{m+1}-z'\right)}\cdot\mathbf{S}_d\end{matrix}\right] \tag{35}$$

When $z' < z < d_{\mathrm{m+1}}$, expressions of up- and down-traveling waves can be similarly obtained:

$$\phi_u = e^{i\bar{\mathbf{\Lambda}}_1^{(m)}(d_{m+1}-z)}\cdot\mathbf{Q}_u \tag{36}$$

$$\phi_d = e^{-i\bar{\mathbf{\Lambda}}_2^{(m)}\left(z-z'\right)}\cdot\mathbf{S}_d + e^{-i\bar{\mathbf{\Lambda}}_2^{(m)}(z-d_m)}\cdot\mathbf{Q}_d \tag{37}$$

(2). The source (m-layer) and receiver (n-layer) are not in the same layer and $m > n$

If $\mathbf{B}_u^{(n)}$ is defined as the amplitude of the up-traveling wave at the interface d_{n+1} as shown in Figure 3, then the up- and down-traveling waves at z can be written as:

$$\phi_u = e^{i\bar{\mathbf{\Lambda}}_1^{(n)}(d_{n+1}-z)}\mathbf{B}_u^{(n)} \tag{38}$$

$$\phi_d = e^{-i\bar{\mathbf{\Lambda}}_2^{(n)}(z-d_n)}\tilde{\bar{\mathbf{R}}}_{n,n-1}e^{i\bar{\mathbf{\Lambda}}_1^{(n)}h_n}\mathbf{B}_u^{(n)} \tag{39}$$

According to the physical characteristics of wave propagation, $\mathbf{B}_u^{(n)}$ is equal to the sum of the transmitted wave $\mathbf{B}'_{u^{(n)}}$ of the up-traveling wave in $n+1$ layer and the reflected wave $\mathbf{B}''_{u^{(n)}}$ of the down-traveling wave in n layer with the following expressions:

$$\mathbf{B}'_{u^{(n)}} = \bar{\mathbf{T}}_{n+1,n}e^{i\bar{\mathbf{\Lambda}}_1^{(n+1)}h_{n+1}}\mathbf{B}_u^{(n+1)} \tag{40}$$

$$\mathbf{B}''_{u^{(n)}} = \bar{\mathbf{R}}_{n,n+1}e^{-i\bar{\mathbf{\Lambda}}_2^{(n)}h_n}\tilde{\bar{\mathbf{R}}}_{n,n-1}e^{i\bar{\mathbf{\Lambda}}_1^{(n)}h_n}\mathbf{B}_u^{(n)} \tag{41}$$

Then, $\mathbf{B}_u^{(n)}$ can be expressed as:

$$\mathbf{B}_u^{(n)} = \left[\bar{\mathbf{I}}-\bar{\mathbf{R}}_{n,n+1}e^{-i\bar{\mathbf{\Lambda}}_2^{(n)}h_n}\tilde{\bar{\mathbf{R}}}_{n,n-1}e^{i\bar{\mathbf{\Lambda}}_1^{(n)}h_n}\right]^{-1}\cdot\bar{\mathbf{T}}_{n+1,n}e^{i\bar{\mathbf{\Lambda}}_1^{(n+1)}h_{n+1}}\mathbf{B}_u^{(n+1)} \tag{42}$$

Using (42), $\mathbf{B}_u^{(n)}$ can be calculated recursively from the amplitude $\mathbf{B}_u^{(m-1)}$ of $m-1$ layer, and the expression of $\mathbf{B}_u^{(m-1)}$ can be obtained similarly to the derivation of $\mathbf{Q}_u$:

$$\mathbf{B}_u^{(m-1)} = \bar{\mathbf{T}}_{m,m-1}\left[\bar{\mathbf{I}}-e^{i\bar{\mathbf{\Lambda}}_1^{(m)}h_m}\tilde{\bar{\mathbf{R}}}_{m,m+1}e^{-i\bar{\mathbf{\Lambda}}_2^{(m)}h_m}\tilde{\bar{\mathbf{R}}}_{m,m-1}\right]^{-1}\cdot\left[e^{i\bar{\mathbf{\Lambda}}_1^{(m)}h_m}\tilde{\bar{\mathbf{R}}}_{m,m+1}e^{-i\bar{\mathbf{\Lambda}}_2^{(m)}\left(d_{m+1}-z'\right)}\cdot\mathbf{S}_d - e^{i\bar{\mathbf{\Lambda}}_1^{(m)}\left(z'-d_m\right)}\cdot\mathbf{S}_u\right] \tag{43}$$

(3). The source (m-layer) and receiver (n-layer) are not in the same layer and $m < n$

Using the analytical method presented above, the up- and down-traveling waves for the case of $m < n$ can be obtained as follows:

$$\phi_u = e^{i\bar{\mathbf{\Lambda}}_1^{(n)}(d_{n+1}-z)}\tilde{\bar{\mathbf{R}}}_{n,n+1}e^{-i\bar{\mathbf{\Lambda}}_2^{(n)}h_n}\mathbf{B}_d^{(n)} \tag{44}$$

$$\phi_d = e^{-i\bar{\mathbf{\Lambda}}_2^{(n)}(z-d_n)}\cdot\mathbf{B}_d^{(n)} \tag{45}$$

where $\mathbf{B}_d^{(n)}$ can be obtained from the following recursive relation:

$$\mathbf{B}_d^{(n)} = \left[\bar{\mathbf{I}}-\bar{\mathbf{R}}_{n,n-1}e^{i\bar{\mathbf{\Lambda}}_1^{(n)}h_n}\tilde{\bar{\mathbf{R}}}_{n,n+1}e^{-i\bar{\mathbf{\Lambda}}_2^{(n)}h_n}\right]^{-1}\cdot\bar{\mathbf{T}}_{n-1,n}e^{-i\bar{\mathbf{\Lambda}}_2^{(n-1)}h_{n-1}}\mathbf{B}_d^{(n-1)} \tag{46}$$

It should be noted that, for the case where the source and receiver are not in the same layer, the wave amplitudes on the interfaces d_{n+1} (for $m > n$) and d_n (for $m < n$) are obtained through the recursion formulae given in this study and then used to calculate EM fields, while the wave amplitudes at the interfaces d_n (for $m > n$) and d_{n+1} (for $m < n$) are obtained through the recursion formulae given in the existing literature. Evidently, the recursion formulae proposed in this study are more consistent with the actual physical process of wave propagation.

2.3. Reflection and Transmission at Interface

In the expressions of the EM fields given in the above section, $\tilde{\bar{\mathbf{R}}}_{n,n+1}$ and $\tilde{\bar{\mathbf{R}}}_{n,n-1}$ represent the generalized reflection matrices of the interface and include the contributions of reflection and transmission from the interface of all layers from the source to the receiver. In this section, $\tilde{\bar{\mathbf{R}}}_{n,n+1}$ is chosen as an example to provide recursion derivation. Assuming that a wave with unit size is reflected by d_{n+1}, as shown in Figure 4, and $\tilde{\bar{\mathbf{R}}}_{n,n+1}$ can be expressed as the sum of multiple reflections as follows [5]:

$$\tilde{\bar{\mathbf{R}}}_{n,n+1} = \tilde{\bar{\mathbf{R}}}_{n,n+1}^{(0)}+\tilde{\bar{\mathbf{R}}}_{n,n+1}^{(1)}+\tilde{\bar{\mathbf{R}}}_{n,n+1}^{(2)}+\tilde{\bar{\mathbf{R}}}_{n,n+1}^{(3)}+\ldots \tag{47}$$

According to the process of wave propagation in Figure 4, the expression of each term in (47) can be written as (owing to space constraints, only the first three terms are presented here):

$$\tilde{\bar{\mathbf{R}}}_{n,n+1}^{(0)} = \bar{\mathbf{R}}_{n,n+1} \tag{48}$$

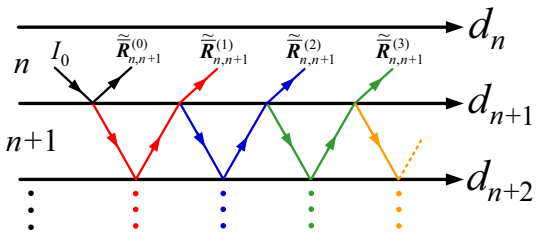

FIGURE 4. Schematic diagram of multiple reflections for waves in the HMLM.

$$\tilde{\bar{\mathbf{R}}}^{(1)}_{n,n+1}=\bar{\mathbf{T}}_{n+1,n}e^{i\bar{\mathbf{\Lambda}}_1^{(n+1)}h_{n+1}}\tilde{\bar{\mathbf{R}}}_{n+1,n+2}e^{-i\bar{\mathbf{\Lambda}}_2^{(n+1)}h_{n+1}}\bar{\mathbf{T}}_{n,n+1} \quad (49)$$

$$\tilde{\bar{\mathbf{R}}}^{(2)}_{n,n+1}=\begin{Bmatrix}\bar{\mathbf{T}}_{n+1,n}e^{i\bar{\mathbf{\Lambda}}_1^{(n+1)}h_{n+1}}\tilde{\bar{\mathbf{R}}}_{n+1,n+2}e^{-i\bar{\mathbf{\Lambda}}_2^{(n+1)}h_{n+1}}\bar{\mathbf{R}}_{n+1,n}\\ \cdot\left[e^{i\bar{\mathbf{\Lambda}}_1^{(n+1)}h_{n+1}}\tilde{\bar{\mathbf{R}}}_{n+1,n+2}e^{-i\bar{\mathbf{\Lambda}}_2^{(n+1)}h_{n+1}}\bar{\mathbf{T}}_{n,n+1}\right]\end{Bmatrix} \quad (50)$$

$$\tilde{\bar{\mathbf{R}}}^{(3)}_{n,n+1}=\begin{Bmatrix}\bar{\mathbf{T}}_{n+1,n}e^{i\bar{\mathbf{\Lambda}}_1^{(n+1)}h_{n+1}}\tilde{\bar{\mathbf{R}}}_{n+1,n+2}e^{-i\bar{\mathbf{\Lambda}}_2^{(n+1)}h_{n+1}}\bar{\mathbf{R}}_{n+1,n}\\ \cdot\begin{bmatrix}e^{i\bar{\mathbf{\Lambda}}_1^{(n+1)}h_{n+1}}\tilde{\bar{\mathbf{R}}}_{n+1,n+2}e^{-i\bar{\mathbf{\Lambda}}_2^{(n+1)}h_{n+1}}\bar{\mathbf{R}}_{n+1,n}\\ \cdot e^{i\bar{\mathbf{\Lambda}}_1^{(n+1)}h_{n+1}}\tilde{\bar{\mathbf{R}}}_{n+1,n+2}e^{-i\bar{\mathbf{\Lambda}}_2^{(n+1)}h_{n+1}}\bar{\mathbf{T}}_{n,n+1}\end{bmatrix}\end{Bmatrix} \quad (51)$$

Substituting (48)–(51) into (47), $\tilde{\bar{\mathbf{R}}}_{n,n+1}$ can be expressed as:

$$\begin{aligned}\tilde{\bar{\mathbf{R}}}_{n,n+1}&=\bar{\mathbf{R}}_{n,n+1}+\bar{\mathbf{T}}_{n+1,n}e^{i\bar{\mathbf{\Lambda}}_1^{(n+1)}h_{n+1}}\tilde{\bar{\mathbf{R}}}_{n+1,n+2}\\&\quad\cdot\left\{\bar{\mathbf{I}}+\bar{\mathbf{\Gamma}}\left[\bar{\mathbf{I}}+\bar{\mathbf{\Gamma}}\left(\bar{\mathbf{I}}+\bar{\mathbf{\Gamma}}\langle\bar{\mathbf{I}}+\ldots\rangle\right)\right]\right\}e^{-i\bar{\mathbf{\Lambda}}_2^{(n+1)}h_{n+1}}\bar{\mathbf{T}}_{n,n+1}\\&=\bar{\mathbf{R}}_{n,n+1}+\begin{Bmatrix}\bar{\mathbf{T}}_{n+1,n}e^{i\bar{\mathbf{\Lambda}}_1^{(n+1)}h_{n+1}}\tilde{\bar{\mathbf{R}}}_{n+1,n+2}\\ \cdot\begin{bmatrix}\bar{\mathbf{I}}-e^{-i\bar{\mathbf{\Lambda}}_2^{(n+1)}h_{n+1}}\bar{\mathbf{R}}_{n+1,n}\\ e^{i\bar{\mathbf{\Lambda}}_1^{(n+1)}h_{n+1}}\tilde{\bar{\mathbf{R}}}_{n+1,n+2}\end{bmatrix}^{-1}\\ e^{-i\bar{\mathbf{\Lambda}}_2^{(n+1)}h_{n+1}}\bar{\mathbf{T}}_{n,n+1}\end{Bmatrix}\end{aligned} \quad (52)$$

where $\bar{\Gamma}=e^{-i\bar{\mathbf{\Lambda}}_2^{(n+1)}h_{n+1}}\bar{\mathbf{R}}_{n+1,n}e^{i\bar{\mathbf{\Lambda}}_1^{(n+1)}h_{n+1}}\tilde{\bar{\mathbf{R}}}_{n+1,n+2}$.

Similarly, the expression of $\tilde{\bar{\mathbf{R}}}_{n,n-1}$ can also be obtained:

$$\begin{aligned}\tilde{\bar{\mathbf{R}}}_{n,n-1}&=\bar{\mathbf{R}}_{n,n-1}\\&\quad+\begin{Bmatrix}\bar{\mathbf{T}}_{n-1,n}e^{-i\bar{\mathbf{\Lambda}}_2^{(n-1)}h_{n-1}}\tilde{\bar{\mathbf{R}}}_{n-1,n-2}\\ \cdot\begin{bmatrix}\bar{\mathbf{I}}-e^{i\bar{\mathbf{\Lambda}}_1^{(n-1)}h_{n-1}}\bar{\mathbf{R}}_{n-1,n}\\ e^{-i\bar{\mathbf{\Lambda}}_2^{(n-1)}h_{n-1}}\tilde{\bar{\mathbf{R}}}_{n-1,n-2}\end{bmatrix}^{-1}\\ e^{i\bar{\mathbf{\Lambda}}_1^{(n-1)}h_{n-1}}\bar{\mathbf{T}}_{n,n-1}\end{Bmatrix}\end{aligned} \quad (53)$$

In (52)–(53), $\bar{\mathbf{R}}_{n,n+1}$, $\bar{\mathbf{R}}_{n,n-1}$, $\bar{\mathbf{T}}_{n,n+1}$, and $\bar{\mathbf{T}}_{n,n-1}$ represent the reflection and transmission matrices of a single interface, which can be obtained from the boundary conditions of the EM fields at the interface [23].

2.4. Analytical Solutions of Eigenvalues and Eigenvectors

It can be seen from the above analysis that to express the EM fields in WD, it is also necessary to calculate the eigenvalues and eigenvectors of the coefficient matrix $\bar{\mathbf{K}}$. According to matrix theory [27], the eigenvalues of $\bar{\mathbf{K}}$ satisfy the following quartic equation:

$$\lambda^4+a_3\lambda^3+a_2\lambda^2+a_1\lambda+a_0=0 \quad (54)$$

where,

$$a_3=-\left(K_{11}+K_{22}+K_{33}+K_{44}\right) \quad (55)$$

$$a_2=\begin{bmatrix}K_{11}K_{22}+K_{33}K_{44}+(K_{11}+K_{22})(K_{33}+K_{44})\\ -K_{12}K_{21}-K_{13}K_{31}-K_{14}K_{41}\\ -K_{23}K_{32}-K_{24}K_{42}-K_{34}K_{43}\end{bmatrix} \quad (56)$$

$$a_1=\begin{bmatrix}-K_{11}K_{22}\left(K_{33}+K_{44}\right)-K_{33}K_{44}\left(K_{11}+K_{22}\right)\\ +K_{12}K_{21}\left(K_{33}+K_{44}\right)+K_{13}K_{31}\left(K_{22}+K_{44}\right)\\ +K_{14}K_{41}\left(K_{22}+K_{33}\right)+K_{23}K_{32}\left(K_{11}+K_{44}\right)\\ +K_{24}K_{42}\left(K_{11}+K_{33}\right)+K_{34}K_{43}\left(K_{11}+K_{22}\right)\\ -K_{23}K_{34}K_{42}-K_{13}K_{21}K_{32}-K_{14}K_{31}K_{43}\\ -K_{12}K_{24}K_{41}-K_{24}K_{32}K_{43}-K_{14}K_{21}K_{42}\\ -K_{12}K_{23}K_{31}-K_{13}K_{34}K_{41}\end{bmatrix} \quad (57)$$

$$a_0=\begin{pmatrix}K_{11}K_{22}K_{33}K_{44}+K_{12}K_{21}K_{34}K_{43}\\ -K_{12}K_{23}K_{34}K_{41}+K_{13}K_{24}K_{31}K_{42}\\ +K_{14}K_{23}K_{32}K_{41}-K_{14}K_{21}K_{32}K_{43}\\ -K_{13}K_{24}K_{32}K_{41}-K_{14}K_{23}K_{31}K_{42}\\ -K_{12}K_{24}K_{31}K_{43}-K_{13}K_{21}K_{34}K_{42}\\ -K_{24}K_{42}K_{11}K_{33}-K_{13}K_{31}K_{22}K_{44}\\ +K_{11}K_{23}K_{34}K_{42}-K_{34}K_{43}K_{11}K_{22}\\ +K_{44}K_{13}K_{21}K_{32}+K_{14}K_{31}K_{43}K_{22}\\ +K_{33}K_{12}K_{24}K_{41}-K_{12}K_{21}K_{33}K_{44}\\ +K_{11}K_{24}K_{32}K_{43}-K_{23}K_{32}K_{11}K_{44}\\ +K_{14}K_{21}K_{42}K_{33}-K_{14}K_{41}K_{22}K_{33}\\ +K_{44}K_{12}K_{23}K_{31}+K_{22}K_{13}K_{34}K_{41}\end{pmatrix} \quad (58)$$

The quartic equation (54) can be solved using the Ferrari method [28], and four eigenvalues can be obtained:

$$\lambda=\frac{-\alpha\pm\sqrt{\alpha^2-4\beta}}{2} \quad (59)$$

where,

$$\alpha=\frac{a_3}{2}\mp\sqrt{\frac{a_3^2}{4}-a_2+\gamma};\quad \beta=\frac{\gamma}{2}\mp\sqrt{-a_0+\frac{\gamma^2}{4}} \quad (60)$$

In (60), γ satisfies the following cubic equation:

$$\gamma^3-a_2\gamma^2+\left(a_1a_3-4a_0\right)\gamma-\left(a_1^2+a_0a_3^2-4a_0a_2\right)=0 \quad (61)$$

Solutions of Eq. (61) can be easily written as:

$$\gamma=\left(p_2+\sqrt{p_1^3+p_2^2}\right)^{\frac{1}{3}}+\left(p_2-\sqrt{p_1^3+p_2^2}\right)^{\frac{1}{3}}-\frac{a_2}{3} \quad (62)$$

where,

$$p_1=\frac{1}{3}\left(a_1a_3-4a_0\right)-\frac{1}{9}a_2^2 \quad (63)$$

$$p_2=\frac{1}{6}\left[\left(4a_0-a_1a_3\right)a_2-3\left(a_1^2+a_0a_3^2-4a_0a_2\right)\right]+\frac{1}{27}a_2^3 \quad (64)$$

Then, the eigenvector corresponding to each eigenvalue can be calculated by substituting the eigenvalue into $\bar{\mathbf{K}}=\bar{\mathbf{A}}\cdot\bar{\mathbf{\Lambda}}\cdot\bar{\mathbf{A}}^{-1}$ and is expressed as:

$$A_{2j}=\left(K_{31}K_{24}-K_{21}K_{34}\right)\left[K_{41}\left(K_{33}-\lambda_j\right)-K_{31}K_{43}\right]$$

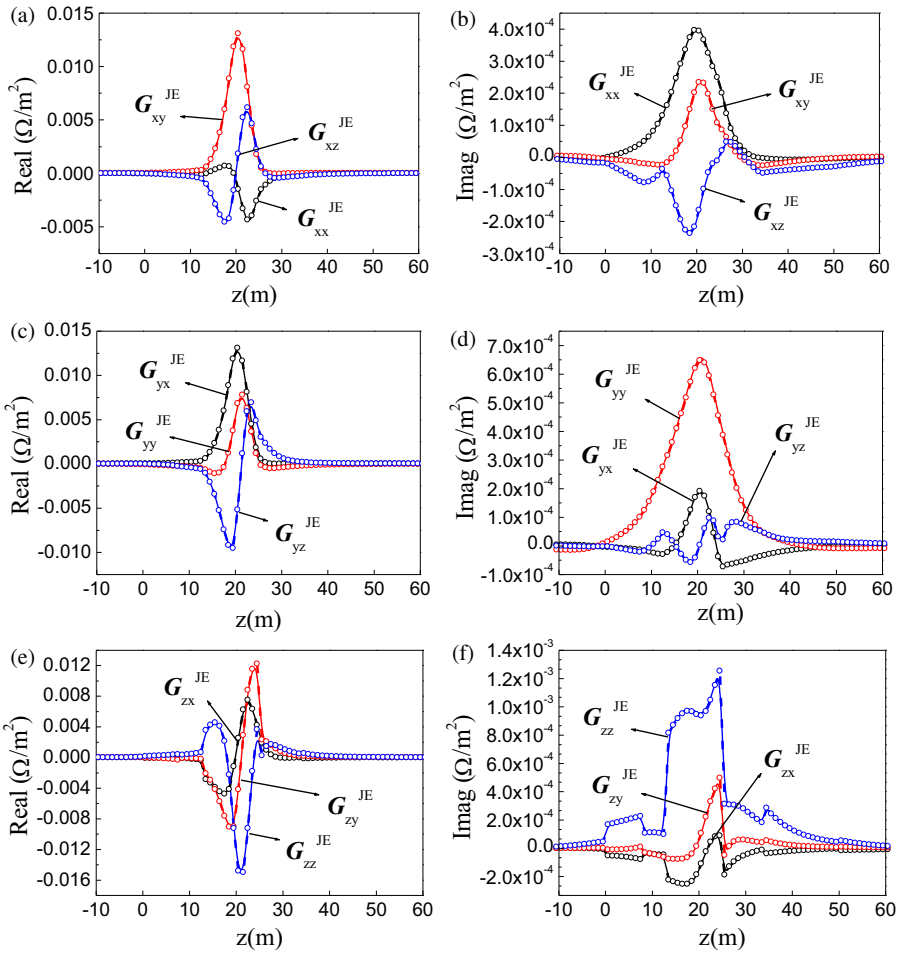

FIGURE 5. Distributions of $\bar{G}^{JE}(\mathbf{r},\mathbf{r}')$ along z-direction (the solid line, circle, and dash represent the results from method of this paper, direct numerical integration, and FVM, respectively).

$$-[K_{41}K_{34}-K_{31}(K_{44}-\lambda_j)][K_{31}K_{23}-K_{21}(K_{33}-\lambda_j)] \quad (65)$$

$$A_{3j}=[K_{31}(K_{22}-\lambda_j)-K_{21}K_{32}][K_{41}K_{34}-K_{31}(K_{44}-\lambda_j)] - (K_{41}K_{32}-K_{31}K_{42})(K_{31}K_{24}-K_{21}K_{34}) \quad (66)$$

$$A_{4j}=(K_{41}K_{32}-K_{31}K_{42})[K_{31}K_{23}-K_{21}(K_{33}-\lambda_j)] -[K_{31}(K_{22}-\lambda_j)-K_{21}K_{32}][K_{41}(K_{33}-\lambda_j)-K_{31}K_{43}] \quad (67)$$

$$A_{1j}=-(K_{12}A_{2j}+K_{13}A_{3j}+K_{14}A_{4j})/(K_{11}-\lambda_j) \quad (68)$$

here $j = 1, 2, 3, 4$.

2.5. EM Fields in the SD

To obtain the EM fields in the SD, the EM fields in the WD must be subjected to a 2-D inverse Fourier transform:

$$f(x-x',y-y';z,z') = \frac{1}{4\pi^2}\iint_{-\infty}^{+\infty}\tilde{f}(k_x,k_y;z,z')e^{i[k_x(x-x')+k_y(y-y')]}dk_xdk_y \quad (69)$$

It can be predicted that the efficiency of using direct numerical integration to evaluate the above 2-D infinite integral is relatively low. To accelerate the numerical integration, based on Euler's formula, the infinite integral (69) can be transformed into the following four semi-infinite integrals:

$$\begin{aligned}
&\frac{1}{4\pi^2}\times f(x-x',y-y';z,z') \\
&=\iint_0^{+\infty}\tilde{f}_1(k_x,k_y;z,z')\cos[k_x|x-x'|]\cos[k_y|y-y'|]\,dk_xdk_y \\
&+\begin{bmatrix}\Theta(x-x')\\ \cdot\Theta(y-y')\end{bmatrix}\cdot\iint_0^{+\infty}\begin{Bmatrix}\tilde{f}_2(k_x,k_y;z,z')\\ \cdot\sin[k_x|x-x'|]\\ \sin[k_y|y-y'|]\end{Bmatrix}dk_xdk_y \\
&+i\Theta(y-y')\iint_0^{+\infty}\begin{Bmatrix}\tilde{f}_3(k_x,k_y;z,z')\\ \cdot\cos[k_x|x-x'|]\\ \sin[k_y|y-y'|]\end{Bmatrix}dk_xdk_y \\
&+i\Theta(x-x')\iint_0^{+\infty}\begin{Bmatrix}\tilde{f}_4(k_x,k_y;z,z')\\ \cdot\sin[k_x|x-x'|]\\ \cos[k_y|y-y'|]\end{Bmatrix}dk_xdk_y
\end{aligned} \quad (70)$$

where $\Theta(\eta-\eta')=\begin{cases}1(\eta>\eta')\\ 0(\eta<\eta')\end{cases}$ $(\eta=x,y)$ and,

$\tilde{f}_1(k_x,k_y)$

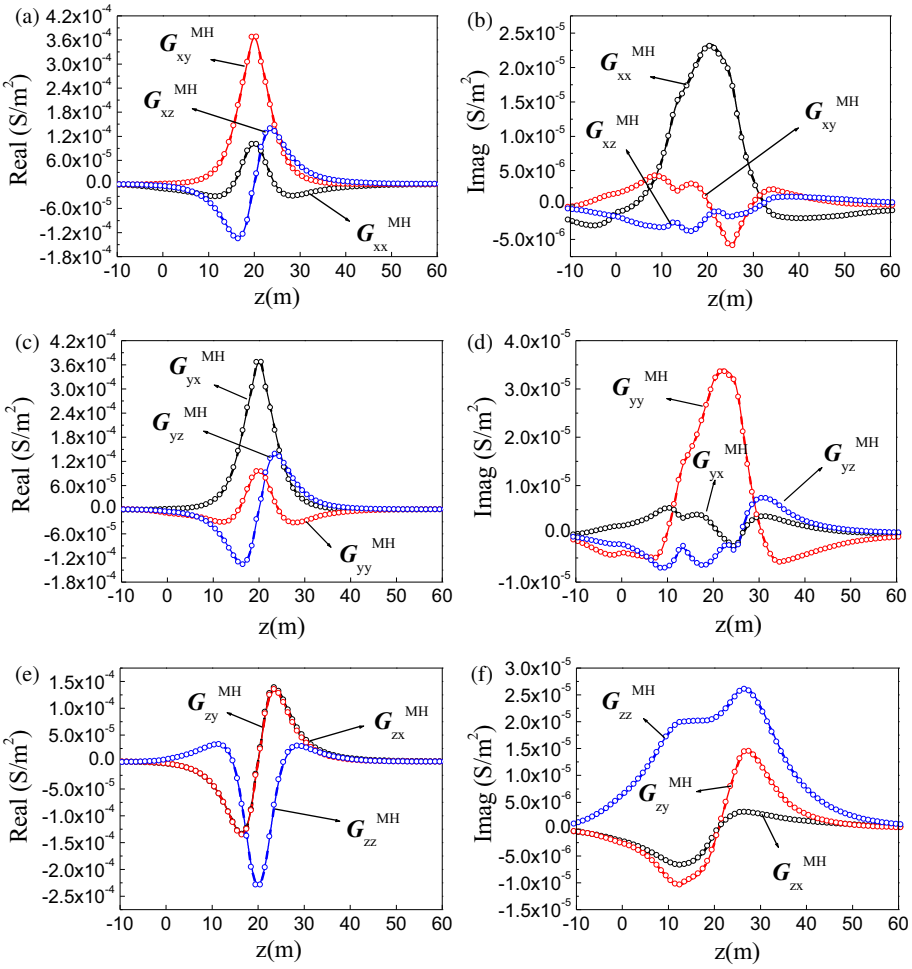

FIGURE 6. Distributions of $\bar{G}^{MH}(\mathbf{r},\mathbf{r}')$ along z-direction (the solid line, circle, and dash represent the results from the method of this paper, direct numerical integration, and FVM, respectively).

$$=\tilde{f}(k_x,k_y)+\tilde{f}(-k_x,k_y)+\tilde{f}(k_x,-k_y)+\tilde{f}(-k_x,-k_y) \quad (71)$$

$$\tilde{f}_2(k_x,k_y)$$

$$=-\tilde{f}(k_x,k_y)+\tilde{f}(-k_x,k_y)+\tilde{f}(k_x,-k_y)-\tilde{f}(-k_x,-k_y) \quad (72)$$

$$\tilde{f}_3(k_x,k_y)$$

$$=\tilde{f}(k_x,k_y)+\tilde{f}(-k_x,k_y)-\tilde{f}(k_x,-k_y)-\tilde{f}(-k_x,-k_y) \quad (73)$$

$$\tilde{f}_4(k_x,k_y)$$

$$=\tilde{f}(k_x,k_y)-\tilde{f}(-k_x,k_y)+\tilde{f}(k_x,-k_y)-\tilde{f}(-k_x,-k_y) \quad (74)$$

Integrals (70) can be evaluated by introducing fast Fourier sine and cosine transforms based on a digital filter algorithm [29]. The filter coefficients are designed using the following two integral identities

$$\int_0^\infty x^2 e^{-a^2x^2}\cos(bx)\,dx=\sqrt{\pi}\left(\frac{2a^2-b^2}{8a^5}\right)e^{-\left(b^2/4a^2\right)} \quad (75)$$

$$\int_0^\infty x^3 e^{-a^2x^2}\sin(bx)\,dx=\sqrt{\pi}\left(\frac{6ba^2-b^3}{16a^7}\right)e^{-\left(b^2/4a^2\right)} \quad (76)$$

Taking the third integral in (70) as an example, its value can be evaluated by

$$\iint_0^{+\infty}\tilde{f}_3(k_x,k_y;z,z')\cos[k_x|x-x'|]\sin[k_y|y-y'|]dk_xdk_y$$

$$=\frac{\sum_{i=N_1}^{N_2}\sum_{j=M_1}^{M_2}W_i^cW_j^s\tilde{f}_3\left(e^{A_i-\ln|x-x'|},e^{B_j-\ln|y-y'|};z,z'\right)}{|x-x'|\cdot|y-y'|} \quad (77)$$

where A_i and B_j are the corresponding equally spaced filter abscissas, and W_i^c and W_j^s are the 151 filter coefficients sampled with 0.1 in the log-space designed in advance.

3. NUMERICAL VERIFICATION

Considering an HMLM model with a seven-layered medium, as shown in Figure 1, it is assumed that the top- and bottom-layers are half-space, and the boundary positions of other layers are $d_2d_3,\cdots,d_7=0,8,13,25,34,50\,\mathrm{m}$, respectively. Since the application background of this work primarily involves forward modeling of geophysical electromagnetic problems and

TABLE 1. Conductivity tensor of the designed HMLM.

Layer	σ_{xx}	σ_{xy}	σ_{xz}	σ_{yx}	σ_{yy}	σ_{yz}	σ_{zx}	σ_{zy}	σ_{zz}
1	0.83	0.19	0.26	0.19	0.39	0.043	0.26	0.043	0.32
2	0.091	0.0014	0.02	0.0014	0.118	−0.019	0.02	−0.019	0.066
3	0.29	0.056	0.048	0.056	0.126	0.04	0.048	0.04	0.18
4	0.057	0.01	0.015	0.01	0.0356	7.2E-4	0.015	7.2E-4	0.0275
5	0.4	0.11	0.14	0.11	0.13	0.032	0.14	0.032	0.11
6	0.16	0.041	0.057	0.041	0.073	6.8E-3	0.057	6.8E-3	0.052
7	0.08	0.023	0.029	0.023	0.027	6.5E-3	0.029	6.5E-3	0.023

considering that general stratigraphic structures possess non-magnetic properties, the permeability $\bar{\mu}$ in the following calculations is thus assumed to be a unit tensor. On the other hand, given that the working frequency in geo-electromagnetism is generally below 10 kHz and as it is conventional to neglect the effect of displacement current [4], the permittivity tensor $\bar{\varepsilon}$ is therefore assumed to be a zero tensor in the following calculations. Based on the aforementioned considerations, the dominant medium parameter in Maxwell's equations (2) is the conductivity within the complex permittivity expression, which is assumed to take a fully anisotropic form as shown in Table 1 (the unit of conductivity is S/m in the table). Additionally, let the source be located at $(x', y', z') = (0, 0, 20\,\mathrm{m})$, the transverse coordinate of the receiver be $x = y = 5\,\mathrm{m}$, and the working frequency be 10 kHz.

The DGFs for electric and magnetic fields are calculated from $-10\,\mathrm{m}$ to $60\,\mathrm{m}$ along z-axis using the method in this paper, the direct numerical integration [30], and the finite volume method (FVM) in [31], as shown in (a)–(f) of Figures 5–6. Here, the solid line, circle, and dash represent the results calculated by the method proposed in this paper, direct numerical integration, and FVM, respectively. It can be seen that the calculation results of the three methods are in good agreement for all components of DGFs. From the perspective of computation time, all the curves in the figure contain 75 points. When they are tested on the same computer (Intel Core i7-13700H CPU @ 2.40 GHz, 32 GB RAM), the computation times are 7.5, 152.1, and 289.3 seconds, respectively. It can be observed that while maintaining computational accuracy, the proposed method exhibits higher computational efficiency than the other two methods.

In addition, several numerical experiments were conducted to ensure the correctness and accuracy of the proposed method. Owing to space limitations, no specific numerical verification results are presented here.

4. CONCLUSIONS

In this study, a semi-analytical method is proposed for the calculation of EM fields in HMLM with full anisotropy. The governing equation was obtained by plane wave decomposition of Maxwell's equations, and the EM fields in the WD were solved by introducing eigen systems. A more intuitive derivation of the propagation matrix method based on existing literature was used to obtain the EM fields in the HMLM. EM fields in the SD were obtained using a 2-D inverse Fourier transform, and the fast sine(cosine) transforms based on digital filters were introduced to accelerate the numerical evaluation of the EM fields in the SD. Numerical comparisons with the existing algorithm demonstrate that the proposed method can be effectively used to calculate the EM fields in the HMLM with full anisotropy.

This method can be applied to the simulation and analysis of EM characteristics in anisotropic inhomogeneous media, and can also provide the necessary 1-D background field computation method for MOM simulations of EM scattering from 3-D targets buried in anisotropic media.

ACKNOWLEDGEMENT

This work was supported by the projects of Jilin Provincial Natural Science Foundation under Grant 20210101186JC.

REFERENCES

[1] Kong, J. A., *Electromagnetic Wave Theory*, Wiley, New York, 1990.

[2] Chen, Z. N. and X. Qing, *Substrate-Integrated Millimeter-Wave Antennas for Next-Generation Communication and Radar Systems*, John Wiley & Sons, 2021.

[3] Tsang, L., J. A. Kong, and K.-H. Ding, *Scattering of Electromagnetic Waves: Theories and Applications*, John Wiley & Sons, 2000.

[4] Zhdanov, M. S., *Foundations of Geophysical Electromagnetic Theory and Methods*, Elsevier, 2017.

[5] Chew, W. C., *Waves and Fields in Inhomogenous Media*, IEEE Press, 1995.

[6] Chew, W. C., E. Michielssen, J. M. Song, and J. M. Jin, *Fast and Efficient Algorithms in Computational Electromagnetics*, Artech House, 2001.

[7] Wannamaker, P. E., G. W. Hohmann, and W. A. SanFilipo, "Electromagnetic modeling of three-dimensional bodies in layered earths using integral equations," *Geophysics*, Vol. 49, No. 1, 60–74, 1984.

[8] Graham, J. W. and J. K. Lee, "Reflection and transmission from biaxially anisotropic-isotropic interfaces," *Progress In Electromagnetics Research*, Vol. 136, 681–702, 2013.

[9] Eroglu, A., Y. H. Lee, and J. K. Lee, "Wave propagation and fresnel coefficients for three layered uniaxially anisotropic media with arbitrarily oriented optic axes," *Progress In Electromagnetics Research B*, Vol. 47, 63–86, 2013.

[10] Cui, T. J., W. Wiesbeck, and A. Herschlein, "Electromagnetic scattering by multiple three-dimensional scatterers buried un-

der multilayered media. I. Theory," *IEEE Transactions on Geoscience and Remote Sensing*, Vol. 36, No. 2, 526–534, 1998.

[11] Han, F., J. Zhuo, N. Liu, Y. Liu, H. Liu, and Q. H. Liu, "Fast solution of electromagnetic scattering for 3-D inhomogeneous anisotropic objects embedded in layered uniaxial media by the BCGS-FFT method," *IEEE Transactions on Antennas and Propagation*, Vol. 67, No. 3, 1748–1759, 2019.

[12] Chen, G. B., Y. Zhang, and J. Lu, "Contraction integral equation for modeling of EM scattering by 3-D bodies buried in multilayered anisotropic medium," *IEEE Transactions on Antennas and Propagation*, Vol. 69, No. 2, 962–970, 2021.

[13] Lin, Z. H., Z. Gao, Q. H. Wang, and Y. Li, "Analysis of radiation field excited by a vertical electric dipole in a four-layered region," *Progress In Electromagnetics Research M*, Vol. 95, 35–44, 2020.

[14] Okhmatovski, V. and S. Zheng, *Theory and Computation of Electromagnetic Fields in Layered Media*, John Wiley & Sons, 2024.

[15] Kong, J. A., "Electromagnetic fields due to dipole antennas over stratified anisotropic media," *Geophysics*, Vol. 37, No. 6, 985–996, 1972.

[16] Michalski, K. A. and J. R. Mosig, "Multilayered media Green's functions in integral equation formulations," *IEEE Transactions on Antennas and Propagation*, Vol. 45, No. 3, 508–519, 1997.

[17] Li, X. and L. B. Pedersen, "The electromagnetic response of an azimuthally anisotropic half-space," *Geophysics*, Vol. 56, No. 9, 1462–1473, 1991.

[18] Li, X. and L. B. Pedersen, "Controlled-source tensor magnetotelluric responses of a layered earth with azimuthal anisotropy," *Geophysical Journal International*, Vol. 111, No. 1, 91–103, 1992.

[19] Li, N., D. Hong, W. Han, and Q. H. Liu, "An analytic algorithm for electromagnetic field in planar-stratified biaxial anisotropic formation," *IEEE Transactions on Geoscience and Remote Sensing*, Vol. 58, No. 3, 1644–1653, 2020.

[20] Huang, Y. and J. K. Lee, "Dyadic Green's functions for unbounded and two-layered general anisotropic media," *Progress In Electromagnetics Research B*, Vol. 30, 27–46, 2011.

[21] Yin, C. and H.-M. Maurer, "Electromagnetic induction in a layered earth with arbitrary anisotropy," *Geophysics*, Vol. 66, No. 5, 1405–1416, 2001.

[22] Løseth, L. O. and B. Ursin, "Electromagnetic fields in planarly layered anisotropic media," *Geophysical Journal International*, Vol. 170, No. 1, 44–80, 2007.

[23] Hu, Y., Y. Fang, D. Wang, Y. Zhong, and Q. H. Liu, "Electromagnetic waves in multilayered generalized anisotropic media," *IEEE Transactions on Geoscience and Remote Sensing*, Vol. 56, No. 10, 5758–5766, 2018.

[24] Zeng, S., J. Chen, and X. Hu, "Electromagnetic fields of dipole sources in multilayered arbitrary anisotropic formation," in *2020 IEEE USNC-CNC-URSI North American Radio Science Meeting (Joint with AP-S Symposium)*, 145–146, Montreal, QC, Canada, 2020.

[25] Penninck, L., P. D. Visschere, J. Beeckman, and K. Neyts, "Dipole radiation within one-dimensional anisotropic microcavities: A simulation method," *Optics Express*, Vol. 19, No. 19, 18 558–18 576, 2011.

[26] James, J. F., *A Student's Guide to Fourier Transforms: With Applications in Physics and Engineering*, Cambridge University Press, 2011.

[27] Meyer, C. D., *Matrix Analysis and Applied Linear Algebra*, Society for Industrial and Applied Mathematics, Philadelphia, 2000.

[28] Kurosh, A., *Higher Algebra*, MIR Publishers, Moscow, 1980.

[29] Anderson, W. L., "A hybrid fast hankel transform algorithm for electromagnetic modeling," *Geophysics*, Vol. 54, No. 2, 263–266, 1989.

[30] Dahlquist, G., *Numerical Methods in Scientific Computing: Volume 1*, Society for Industrial and Applied Mathematics, Philadelphia, 2008.

[31] Zhang, Y., H.-N. Wang, H.-G. Tao, and S.-W. Yang, "Finite volume algorithm to simulate 3D responses of multi-component induction tools in inhomogeneous anisotropic formation based on coupled scalar-vector potentials," *Chinese Journal of Geophysics*, Vol. 55, No. 6, 2141–2152, 2012.